PERGAMON

International Journal of Heat and Mass Transfer 43 (2000) 1505–1522

International Journal of HEAT and MASS TRANSFER

www.elsevier.com/locate/ijhmt

Onset of double-diffusive convection in a rectangular porous cavity subject to mixed boundary conditions

A. Mahidjiba, M. Mamou, P. Vasseur*

Ecole Polytechnique, University of Montreal, CP 6079, Succ 'Down Town', Montreal, PQ, Canada H3C 3A7

Received 23 February 1999; received in revised form 16 July 1999

Abstract

The onset of double-diffusive convection in a horizontal porous cavity is studied numerically using linear stability analysis. In the formulation of the problem, use is made of the Darcy model with the Boussinesq approximation. Mixed boundary conditions for heat and solute are specified on the horizontal walls of the enclosure while the two vertical ones are impermeable and adiabatic. The Galerkin and the finite element methods are used to solve the perturbation equations. The onset of convection is found to be dependent of the aspect ratio of the cavity, A, normalized porosity, ε, Lewis number, Le, solutal to thermal buoyancy ratio, N, and the thermal and solutal boundary conditions. For a confined enclosure, it is shown that there exists a supercritical Rayleigh number, R_{TC}^{sup}, for the onset of the supercritical convection and an overstable Rayleigh number, R_{TC}^{over}, at which overstability may arise. Furthermore, the overstable regime is shown to exist up to a critical Rayleigh number, R_{TC}^{osc}, at which the transition from the oscillatory to direct mode convection occurs. However, for an infinite layer ($A \to \infty$) the results indicate the absence of an overstable regime. Numerical results for finite amplitude convection, obtained by solving numerically the full governing equations, demonstrate that subcritical convection is possible.

1. Introduction

Buoyancy-driven instability in a horizontal porous layer saturated by a monocomponent fluid, heated from below in the presence of a gravitational field, has received considerable attention owing to relevance in many natural and industrial problems. Starting with the pioneering works of Horton and Rogers [1] and Lapwood [2], several studies have been devoted to the onset of convection in horizontal porous layers. An excellent review of the available investigations in this domain has been reported by Nield and Bejan [3].

A related phenomenon that has received relatively less attention is the stability of a porous layer saturated by binary-fluids. The resulting flows, induced by both temperature and concentration fields, are expected to be much more complicated than the purely thermal convection flow, especially when the two buoyancies are in opposite directions. The growing research on double-diffusing natural convection in porous media is mainly motivated by its importance in diverse engineering problems such as the migration of moisture in fibrous insulation, the contaminant transport in saturated soil, the underground disposal of nuclear wastes and drying processes.

The onset of double diffusive convection in por-

* Corresponding author. Tel.: +1-514-340-4711; fax: +1-514-340-5917.

E-mail address: vasseur@meca.polymtl.ca (P. Vasseur).

0017-9310/00/$ - see front matter
PII: S0017-9310(99)00238-0

Nomenclature

A	aspect ratio, W'/H'
D	solutal diffusivity
g	acceleration due to gravity
H'	height of the enclosure
k	thermal conductivity of the saturated porous medium
K	permeability of the porous medium
Le	Lewis number, α/D
N_{ey}	number of elements in y-direction
N	buoyancy ratio, $\beta_S\Delta S'/\beta_T\Delta T'$
$\overline{Nu}$	overall Nusselt number, Eq. (35)
q'	uniform heat flux (per unit area)
R_S	solutal Darcy–Rayleigh number, $g\beta_S K\Delta S'H'/D\nu$
R_T	thermal Darcy–Rayleigh number, $g\beta_T K\Delta T'H'/\alpha\nu$
S	dimensionless concentration, $(S'-S'_r)/\Delta S'$
S'_L	higher concentration of the lower wall
S'_U	lower concentration of the upper wall
S'_r	reference concentration, $(S'_L+S'_U)/2$
$\overline{Sh}$	overall Sherwood number, Eq. (35)
t	dimensionless time, $t'\alpha/\sigma H'^2$
T	dimensionless temperature, $(T'-T'_r)/\Delta T'$
T'_r	reference temperature at $x'=y'=0$
u, v	dimensionless velocities in x- and y-directions, $(u', v')H'/\alpha$
W'	width of the enclosure
x, y	dimensionless coordinate system, $(x', y')/H'$

Greek symbols

α	thermal diffusivity, $k/(\rho C)_f$
β_S	solutal expansion coefficient
β_T	thermal expansion coefficient
$\Delta S'$	characteristic concentration, $(S'_L-S'_U)$
$\Delta T'$	characteristic temperature, $q'H'/k$
ε	normalized porosity of the porous medium, $\varepsilon=\Phi/\sigma$
ν	kinematic viscosity of fluid
ρ	density of fluid
$(\rho C)_f$	heat capacity of fluid
$(\rho C)_p$	heat capacity of saturated porous medium
σ	heat capacity ratio, $(\rho C)_p/(\rho C)_f$
Φ	porosity of the porous medium
Ψ	dimensionless stream function, Ψ'/α

Subscripts

C	pure diffusive state
max	maximum value
r	reference state

Superscript

′	dimensionless variable

ous layers was first investigated by Nield [4], on the basis of the linear stability theory. The criteria for the existence of steady and oscillatory thermohaline convection was derived by this author. An extension of the above investigation was made by Taunton and Lightfoot [5] to more completely characterize the onset of convection in an infinite horizontal porous layer stratified by temperature and concentration. A linear stability analysis was carried out by Poulikakos [6] to study double diffusive convection in a horizontal sparsely packed porous layer. The flow in the porous matrix was investigated by using the Brinkman-extended Darcy model, which accounts for friction due to macroscopic shear. Results for a pure viscous fluid and a Darcy (densely packed) porous medium were obtained from his analysis as limiting cases. The effect of anisotropic thermo-convective currents in the presence of Soret and Dufour effects on the critical Rayleigh numbers for both marginal and overstable motions has been studied by Malashetty [7]. It was found that, depending on the thermal and solutal boundary conditions, the thermo-convective currents have a stabilizing effect as well as a destabilizing effect with respect to the case in which these currents are absent.

A few studies concerning finite amplitude convection in a two-component fluid saturated porous layer are also available in the literature. The nonlinear stability of thermohaline convection in a horizontal porous layer heated from below has been considered by Rudraiah et al. [8]. The critical Rayleigh number, for the onset of finite amplitude convection, was derived using a truncated representation of Fourier series. The effects of Prandtl, Lewis and Darcy numbers on convection are discussed by these authors. Brand and Steinberg [9] investigated the nonlinear effects in the convective instability of a binary mixture in a porous medium near threshold. A finite amplitude solution was derived for both the stationary and the oscillatory instabilities and an oscillatory behavior in time for the Nusselt and Sherwood numbers was predicted. Trevisan and Bejan [10] completed a theoretical and numerical study of the mass transfer effected by high Rayleigh Bénard convection in a two-dimensional saturated porous layer heated from below. The theoretical

conclusions of a scale analysis proposed by these authors were found to be in good agreement with their numerical results. An experimental study of double-diffusive convection in a porous medium has been carried out by Murray and Chen [11]. A good agreement for the critical thermal Rayleigh number was obtained between the experiments and linear stability theory. Thermohaline convective flows through porous media heated from below in a square cavity have been studied by Rosenberg and Spera [12] for a variety of boundary and initial conditions on the salinity field. It was demonstrated numerically that the flow dynamic depends strongly on the buoyancy ratio at fixed Rayleigh and Lewis numbers. Nonlinear double-diffusive fingering convection in a horizontal porous medium, in which horizontal periodic boundary conditions are prescribed, has been considered by Chen and Chen [13]. The stability boundaries dividing the regions of different modes of fluid motion have been identified by these authors in terms of the thermal and solutal Rayleigh numbers. Finite amplitude natural convection within an inclined porous layer, heated and salted from sides by uniform fluxes of heat and mass, has been considered by Mamou et al. [14]. For the case of a horizontal enclosure, the existence of subcritical convection was demonstrated numerically and analytically. Recently, the onset and development of convection in a porous layer corresponding to the double-diffusive configuration where the destabilizing agent is the one with a higher diffusivity, has been investigated by Nguyen et al. [15]. It was demonstrated, on the basis of both linear and nonlinear theories, that steady convection can arise at Rayleigh numbers below the supercritical value. This result, indicating the possible development of subcritical steady flows, was confirmed by numerical solutions of the full nonlinear governing equations.

In this paper, we consider double-diffusive convection in a horizontal porous layer with boundary conditions for each component being a combination of flux and fixed-value types. In the first part of the paper linear stability analysis is carried out to determine the critical parameters of the problem and the boundaries defining the regions of direct and overstable modes. The second part of the paper presents numerical results for the flow field, temperature and concentration distributions, and heat and mass transfer rates for finite amplitude convection.

2. Governing equations

The flow configuration under study is a two-dimensional horizontal porous enclosure of height H' and width W' as depicted in Fig. 1. The top and bottom

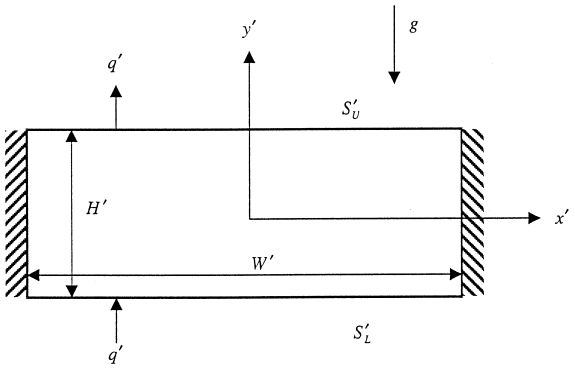

Fig. 1. Flow geometry configuration.

horizontal boundaries are subject to uniform fluxes of heat q', per unit area, which cool and heat, respectively, at the same rate. Also, the lower horizontal wall is maintained at concentration S'_{L}, whereas the upper one is at $S'_{\mathrm{U}} < S'_{\mathrm{L}}$. The two vertical walls are regarded as being insulated and impermeable. The fluid-saturated porous medium is assumed homogeneous and isotropic and inertial effects are neglected. Interaction between the thermal and concentration gradients, known as Soret and Dufour effects, are neglected. The binary fluid that saturates the porous matrix is modeled as a Boussinesq fluid whose density, ρ, varies linearly with temperature, T', and concentration, S',

$$\rho = \rho_{\mathrm{r}}[1 - \beta_{\mathrm{T}}(T' - T'_{\mathrm{r}}) - \beta_{\mathrm{S}}(S' - S'_{\mathrm{r}})] \tag{1}$$

where ρ_{r} is the fluid density at temperature $T' = T'_{\mathrm{r}}$ and concentration $S' = S'_{\mathrm{r}}$, and β_{T} and β_{S} are the thermal and concentration expansion coefficients, respectively. The subscript 'r' denotes a reference state.

The dimensionless equations describing conservation of momentum, energy and constituent in the solution-saturated porous medium are, respectively, given by

$$\nabla^2 \Psi = -R_{\mathrm{T}} \frac{\partial}{\partial x}(T + NS) \tag{2}$$

$$\frac{\partial T}{\partial t} + u\frac{\partial T}{\partial x} + v\frac{\partial T}{\partial y} = \nabla^2 T \tag{3}$$

$$\varepsilon\frac{\partial S}{\partial t} + u\frac{\partial S}{\partial x} + v\frac{\partial S}{\partial y} = \frac{1}{Le}\nabla^2 S \tag{4}$$

where the stream Ψ is defined by

$$u = \frac{\partial \Psi}{\partial y}; \quad v = -\frac{\partial \Psi}{\partial x} \tag{5}$$

such that, the mass conservation is satisfied.

The above equations were nondimensionalized by introducing the following variables.

$$(x, y) = (x', y')/H' \quad (u, v) = (u', v')H'/\alpha$$

$$\Psi = \Psi'/\alpha \quad t = t'\alpha/\sigma H'^2$$

$$T = (T' - T'_r)/\Delta T' \quad S = (S' - S'_r)/\Delta S'$$

$$\Delta T' = q'H'/k \quad \Delta S' = S'_L - S'_U \tag{6}$$

where T'_r is the temperature at the origin of the coordinate system and $S'_r = (S'_L + S'_U)/2$. In the above equations, u and v are the volume-averaged dimensionless velocity components, t the dimensionless time, α, ε and σ the thermal diffusivity of the porous medium, the normalized porosity of the solid matrix, and the porous medium to fluid heat capacity ratio, respectively.

The dimensionless hydrodynamic, thermal and concentration boundary conditions are expressed by

$$x = \pm\frac{A}{2} \quad \Psi = 0 \quad \frac{\partial T}{\partial x} = \frac{\partial S}{\partial x} = 0$$

$$y = \pm\frac{1}{2} \quad \Psi = 0 \quad \frac{\partial T}{\partial y} = -1 \quad S = \pm\frac{1}{2} \tag{7}$$

The non-dimensionalization process results in the appearance of five dimensionless parameters, namely the thermal Darcy–Rayleigh number, R_T, the solutal to thermal buoyancy ratio, N, the Lewis number, Le, the normalized porosity, ε, and the cavity aspect ratio, A defined as

$$R_T = \frac{g\beta_T K\Delta T' H'}{\alpha\nu}; \quad N = \frac{\beta_S \Delta S'}{\beta_T \Delta T'}; \quad Le = \frac{\alpha}{D}; \quad \varepsilon = \frac{\Phi}{\sigma}; \quad A = \frac{W'}{H'} \tag{8}$$

where K is the permeability of the porous medium and D the mass diffusivity.

It is noted that the volumetric expansion coefficient, β_T, due to temperature change is usually positive, but that for concentration change, β_S, can be either positive ($N > 0$) or negative ($N < 0$). With the thermal and solute boundary conditions considered in Fig. 1 it is clear that the thermal gradient is a destabilizing factor while the solute gradient is a destabilizing (stabilizing) one when β_S (i.e., N) is positive (negative). Thus, for $N > 0$, the two buoyancy components make aiding contributions to the overall vertical density distribution while for $N < 0$, they make opposing contributions.

3. Linear stability analysis

In this section the physical situation described by Eqs. (2)–(4), subject to boundary conditions (7), is examined from the standpoint of stability to small perturbations from the rest state. This latter, for which $\Psi = 0$ and heat and mass are transferred via pure diffusion, is a possible solution for the steady state form of the present system. The critical Rayleigh number, above which this no-flow solution becomes unstable, will be now determined on the basis of the linear stability analysis.

We introduce first the following transformation

$$\Psi(t, x, y) = \Psi_C + \psi_0\, e^{pt}\, e^{i\omega x} f(y)$$

$$T(t, x, y) = T_C + \theta_0\, e^{pt}\, e^{i\omega x} g(y)$$

$$S(t, x, y) = S_C + \phi_0\, e^{pt}\, e^{i\omega x} h(y) \tag{9}$$

where the static state of the system is characterized by $\Psi_C = 0$, $T_C = S_C = -y$ and where, as usual, the stream function, temperature and concentration perturbations have been expanded in their normal modes, assuming separability. In the above expressions ψ_0, θ_0 and ϕ_0 are small constant amplitudes and p is the growth rate of the perturbation and ω is defined as $\omega = n\pi/A$ where n is an integer, for a confined enclosure of aspect ratio A. For an infinite layer, $\omega = 2\pi/A_C$ in which A_C is the critical wavelength of the flow configuration.

In Eq. (9) the functions f, g and h describe the vertical perturbation profiles. Thus, they are required to satisfy the following boundary conditions

$$y = \pm\frac{1}{2}; \quad f = \frac{\partial g}{\partial y} = h = 0 \tag{10}$$

Substituting Eq. (9) into Eqs. (2)–(4), after neglecting the small second-order terms, yields the following set of equations

$$\psi_0\left(\frac{\partial^2 f}{\partial y^2} - \omega^2 f\right) = -i\omega R_T(\theta_0 g + N\phi_0 h) \tag{11}$$

$$p\theta_0 g + i\omega\psi_0 f = \theta_0\left(\frac{\partial^2 g}{\partial y^2} - \omega^2 g\right) \tag{12}$$

$$\varepsilon p\phi_0 h + i\omega\psi_0 f = \frac{\phi_0}{Le}\left(\frac{\partial^2 h}{\partial y^2} - \omega^2 h\right) \tag{13}$$

In general the analytical solution of Eqs. (11)–(13), under boundary conditions Eq. (10), is possible but tedious. For this reason the Galerkin finite element

method is used to solve the above linear system of equations.

Using the Green theorem, the variational formulation of Eqs. (11)–(13) yields the following Galerkin integrals

$$\psi_0\int_\Omega\left(\frac{\mathrm{d}f}{\mathrm{d}y}\frac{\mathrm{d}\bar{u}}{\mathrm{d}y}+\omega^2 f\bar{u}\right)\mathrm{d}\Omega = i\omega R_\mathrm{T}\int_\Omega(\theta_0 g+N\phi_0 h)\bar{u}\,\mathrm{d}\Omega \tag{14}$$

$$p\theta_0\int_\Omega g\bar{v}\,\mathrm{d}\Omega+i\omega\psi_0\int_\Omega f\bar{v}\,\mathrm{d}\Omega = -\theta_0\int_\Omega\left(\frac{\mathrm{d}g}{\mathrm{d}y}\frac{\mathrm{d}\bar{v}}{\mathrm{d}y}+\omega^2 g\bar{v}\right)\mathrm{d}\Omega \tag{15}$$

$$\varepsilon p\phi_0\int_\Omega h\bar{w}\,\mathrm{d}\Omega+i\omega\psi_0\int_\Omega f\bar{w}\,\mathrm{d}\Omega = -\frac{\phi_0}{Le}\int_\Omega\left(\frac{\mathrm{d}h}{\mathrm{d}y}\frac{\mathrm{d}\bar{w}}{\mathrm{d}y}+\omega^2 h\bar{w}\right)\mathrm{d}\Omega \tag{16}$$

where $\Omega=[-1/2,\ 1/2]$ and $\bar{u}$, $\bar{v}$ and $\bar{w}$ are admissible shape functions satisfying the boundary conditions in Eq. (10).

In the following sections the conditions for stationary instability will be first discussed. Then, the boundary for oscillatory instability will be delineated. Since the procedure has been described in detail in references [16, 17], only the main steps and the final results will be presented here.

4. Instability via stationary convection ($p = 0$)

The Bubnov–Galerkin procedure, based on the Lagrangian cubic element, is used to solve Eqs. (14)–(16) for the special case $p = 0$ for which the exchange of stability is valid. After assemblage of all the elementary matrices into the global matrices, the following system of space-discretized equations is obtained

$$\psi_0[K_\psi]\{f\} = R_\mathrm{T}[B](\theta_0\{g\}+N\phi_0\{h\}) \tag{17}$$

$$\psi_0[L_\theta]\{f\} = \theta_0[K_\theta]\{g\} \tag{18}$$

$$\psi_0[L_\phi]\{f\} = \frac{\phi_0}{Le}[K_\phi]\{h\} \tag{19}$$

where $[K_\psi]$, $[K_\theta]$, $[K_\phi]$, $[B]$, $[L_\theta]$ and $[L_\phi]$ are $m\times m$ matrices ($m = 2N_{ey}+1$ being the total number of nodes in the discretized domain, and N_{ey} is the number of elements in the y-direction) whose elementary matrices are defined as

$$[K_\psi]^e=\int_{\Delta y^e}\left(\frac{\mathrm{d}N_j}{\mathrm{d}y}\frac{\mathrm{d}N_i}{\mathrm{d}y}+\omega^2 N_jN_i\right)\mathrm{d}y$$

$$[B]^e = i\omega\int_{\Delta y^e}N_jN_i\,\mathrm{d}y$$

$$[K_\psi]^e=[K_\theta]^e=[K_\phi]^e\quad [L_\theta]^e=[L_\psi]^e=-[B]^e$$

where $N_i(y)$ are the Lagrangian shape functions.

Eqs. (17)–(19) can be rearranged to the following canonical eigenvalue problem

$$\psi_0([E]-\lambda[I])\{f\}=0 \tag{20}$$

where I is the identity matrix, $\lambda=1/R_\mathrm{T}$ is the eigenvalue and $[E]$ is given by

$$[E]=[K_\psi]^{-1}[B]([K_\theta]^{-1}[L_\theta]+N\,Le[K_\phi]^{-1}[L_\phi])$$

The functions g and h can be computed from

$$\{g\}=[K_\theta]^{-1}[L_\theta]\{f\}$$

$$\{h\}=[K_\phi]^{-1}[L_\phi]\{f\} \tag{21}$$

The supercritical Rayleigh number for the onset of convection is thus given by

$$R_\mathrm{TC}^\mathrm{sup}=\frac{1}{\lambda_\mathrm{max}} \tag{22}$$

where $\lambda_\mathrm{max}=\max(\lambda_i,\ i=1,\ \ldots,\ m)$ is the maximum eigenvalue.

The precision of the value of $R_\mathrm{TC}^\mathrm{sup}$, predicted by the present finite element method depends naturally on the grid number $m = 2N_{ey}+1$ in the numerical domain. For comparison, typical results are presented in Table 1 for the case of a square cavity heated from below by a constant heat flow ($N\,Le = 0$). For this situation it is observed that a $N_{ey}=15$ mesh size yields an excellent

Table 1
Effect of the grid size on the precision of the computed value of $R_\mathrm{TC}^\mathrm{sup}$ for a square enclosure ($A = 1$) heated from below by a constant heat flux ($N\,Le = 0$)

N_{ey}	5	15	20	Kimura et al. [18]
$R_\mathrm{TC}^\mathrm{sup}$	22.958296	22.946051	22.945940	22.945889
Error (%)	5.4×10^{-2}	7.1×10^{-4}	2.2×10^{-4}	

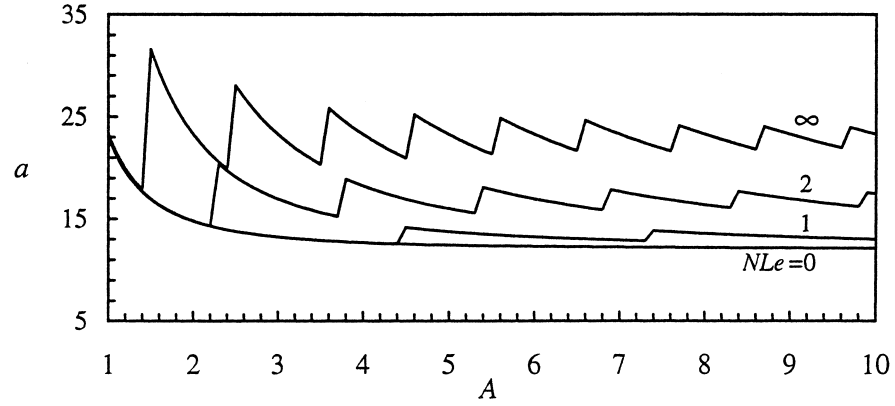

(a)

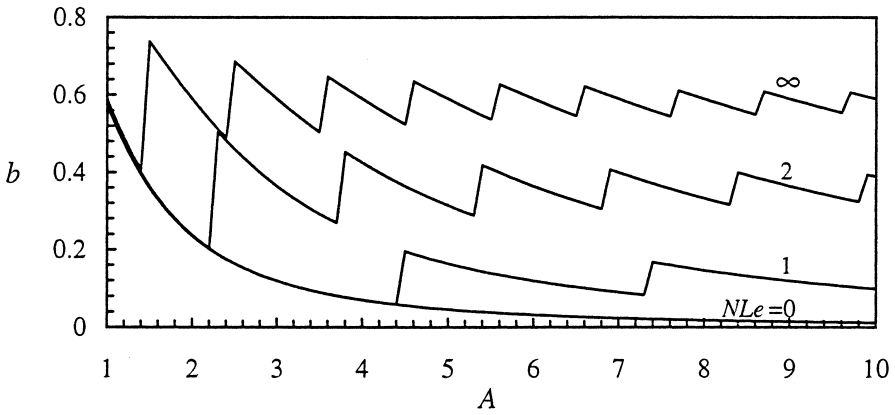

(b)

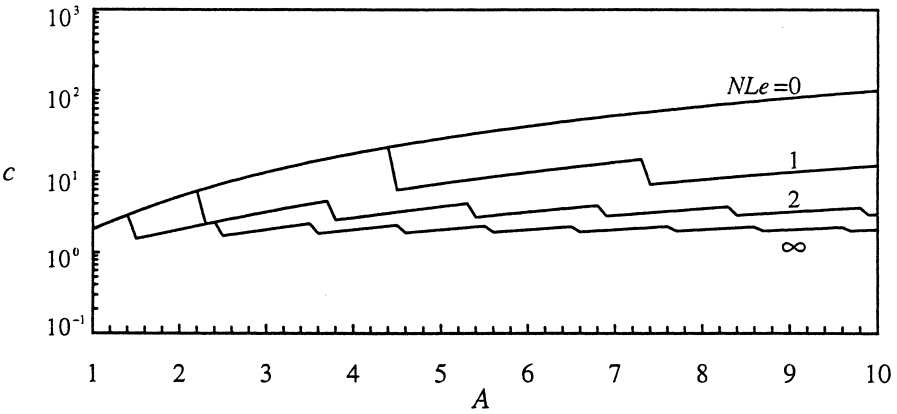

(c)

Fig. 2. Constants *a*, *b* and *c* vs *A* for various values of *N Le*.

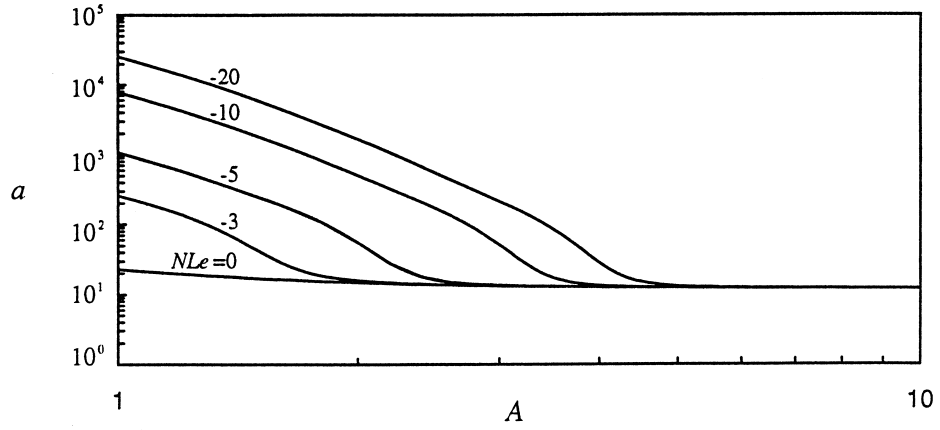

(d)

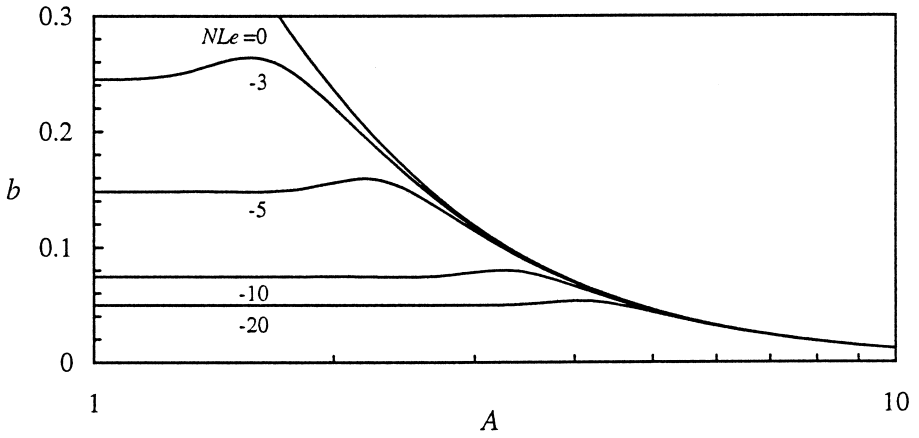

(e)

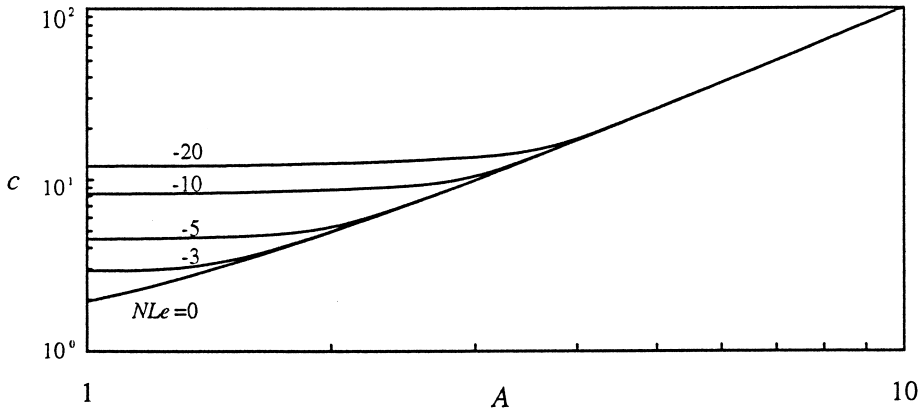

(f)

Fig. 2 (*continued*)

agreement between the numerical results and the analytical solution derived by Kimura et al. [18]. Numerical results concerning the case of an infinite horizontal layer were obtained using the fact that, for this situation, the flow pattern is characterized by the formation of a periodical structure with a given critical wave number, A_C, which depends upon the boundary conditions and the parameter $N\,Le$. Thus, the critical Rayleigh number and wave numbers were predicted numerically in a rectangular channel of aspect ratio A with periodic boundary conditions applied on the vertical boundaries. In this way R_{TC}^{sup} was obtained for various values of A, the minimum value R_{TC}^{sup} being the critical Rayleigh number and the corresponding aspect ratio $A_C = A$ representing the critical wavelength for an infinite horizontal layer. Following this procedure it was found, for instance, that for $N\,Le \to \infty$, $R_{TC}^{sup} = 39.4784/N\,Le$ and $A_C = 1.9996$ in agreement with the classical analytical results $R_{TC}^{sup} = 4\pi^2/N\,Le$ and $A_C = 2$ reported in Ref. [2].

5. Instability via oscillatory convection ($p \neq 0$)

We consider now the marginal state of instability via oscillatory convection for which p is different from zero. Choosing the functions f, g and h as the weighted functions, i.e., $\bar{u} = f$, $\bar{v} = g$ and $\bar{w} = h$, it is readily found from Eqs. (14)–(16) that

$$\psi_0 K_\psi = R_T(\theta_0 B_\theta + N\phi_0 B_\phi) \tag{23}$$

$$p\theta_0 M_\theta - \psi_0 L_\theta = -\theta_0 K_\theta \tag{24}$$

$$\varepsilon p\phi_0 M_\phi - \psi_0 L_\phi = -\frac{\phi_0}{Le} K_\phi \tag{25}$$

where

$$K_\psi = \int_{-1/2}^{1/2} \left[\left(\frac{df}{dy} \right)^2 + \omega^2 f^2 \right] dy; \quad M_\theta = \int_{-1/2}^{1/2} g^2\, dy;$$
$$M_\phi = \int_{-1/2}^{1/2} h^2\, dy$$

$$K_\theta = \int_{-1/2}^{1/2} \left[\left(\frac{dg}{dy} \right)^2 + \omega^2 g^2 \right] dy; \quad B_\theta = i\omega \int_{-1/2}^{1/2} gf\, dy;$$
$$L_\theta = -i\omega \int_{-1/2}^{1/2} fg\, dy$$

$$K_\phi = \int_{-1/2}^{1/2} \left[\left(\frac{dh}{dy} \right)^2 + \omega^2 h^2 \right] dy; \quad B_\phi = i\omega \int_{-1/2}^{1/2} hf\, dy;$$
$$L_\phi = -i\omega \int_{-1/2}^{1/2} fh\, dy \tag{26}$$

Substituting Eqs. (24) and (25) into (23) we get, after some algebra, the following equation for p

$$\varepsilon^2 Le^2 p^2 - \gamma_\theta \varepsilon\, Le\, p_1 p - c\gamma_\theta^2 p_2 = 0 \tag{27}$$

where

$$p_1 = a^{-1} Le\, R_T(\varepsilon + cbN) - (\varepsilon\, Le + c); \quad p_2 = \varepsilon\, Le[a^{-1} R_T(1 + bN\, Le) - 1]$$

$$a = \frac{K_\psi K_\theta}{B_\theta L_\theta}; \quad b = \frac{K_\theta B_\phi L_\phi}{K_\phi B_\theta L_\theta}; \quad c = \frac{\gamma_\phi}{\gamma_\theta}; \quad \gamma_\theta = \frac{K_\theta}{M_\theta}; \quad \gamma_\phi = \frac{K_\phi}{M_\phi} \tag{28}$$

From Eq. (27) it is found that p is given by $p = \gamma_\theta(p_1 \pm \sqrt{p_1^2 + 4cp_2})/(2\varepsilon\, Le)$. The case $p = 0$ corresponds to $p_2 = 0$ for which, according to Eq. (28), the supercritical Rayleigh number, R_{TC}^{sup}, is given by

$$R_{TC}^{sup} = \frac{a}{1 + bN\, Le} \tag{29}$$

In general p is a complex number $p = p_{re} + ip_{im}$, where p_{re} and p_{im} are its real and imaginary parts, respectively. They are given by

$$\left.\begin{aligned} p_{re} &= \frac{\gamma_\theta}{2\varepsilon\, Le}(p_1 \pm \sqrt{p_1^2 + 4cp_2}) \\ p_{im} &= 0 \end{aligned}\right\} \quad \text{if } p_1^2 + 4cp_2 \geq 0 \tag{30}$$

$$\left.\begin{aligned} p_{re} &= \frac{\gamma_\theta P_1}{2\varepsilon\, Le} \\ P_{im} &= \frac{\gamma_\theta}{2\varepsilon\, Le}\sqrt{|\, p_1^2 + 4cp_2\,|} \end{aligned}\right\} \quad \text{if } p_1^2 + 4cp_2 < 0 \tag{31}$$

The overstable critical Rayleigh number, R_{TC}^{over}, corresponds to the condition $p_{re} = 0$, i.e., $p_1 = 0$. From Eq. (28) it is found that

$$R_{TC}^{over} = a\frac{(Le\,\varepsilon + c)}{Le(\varepsilon + bcN)} \tag{32}$$

This Rayleigh number marks the transition from the oscillatory to direct convective modes.

The oscillatory regime $p_{im} \neq 0$ exists only when the condition $p_1^2 + 4cp_2 < 0$ is satisfied, i.e., $R_{TC}^{over} \leq R_T \leq R_{TC}^{osc}$. The value of R_{TC}^{osc} is deduced from the condition $p_1^2 + 4cp_2 = 0$ as

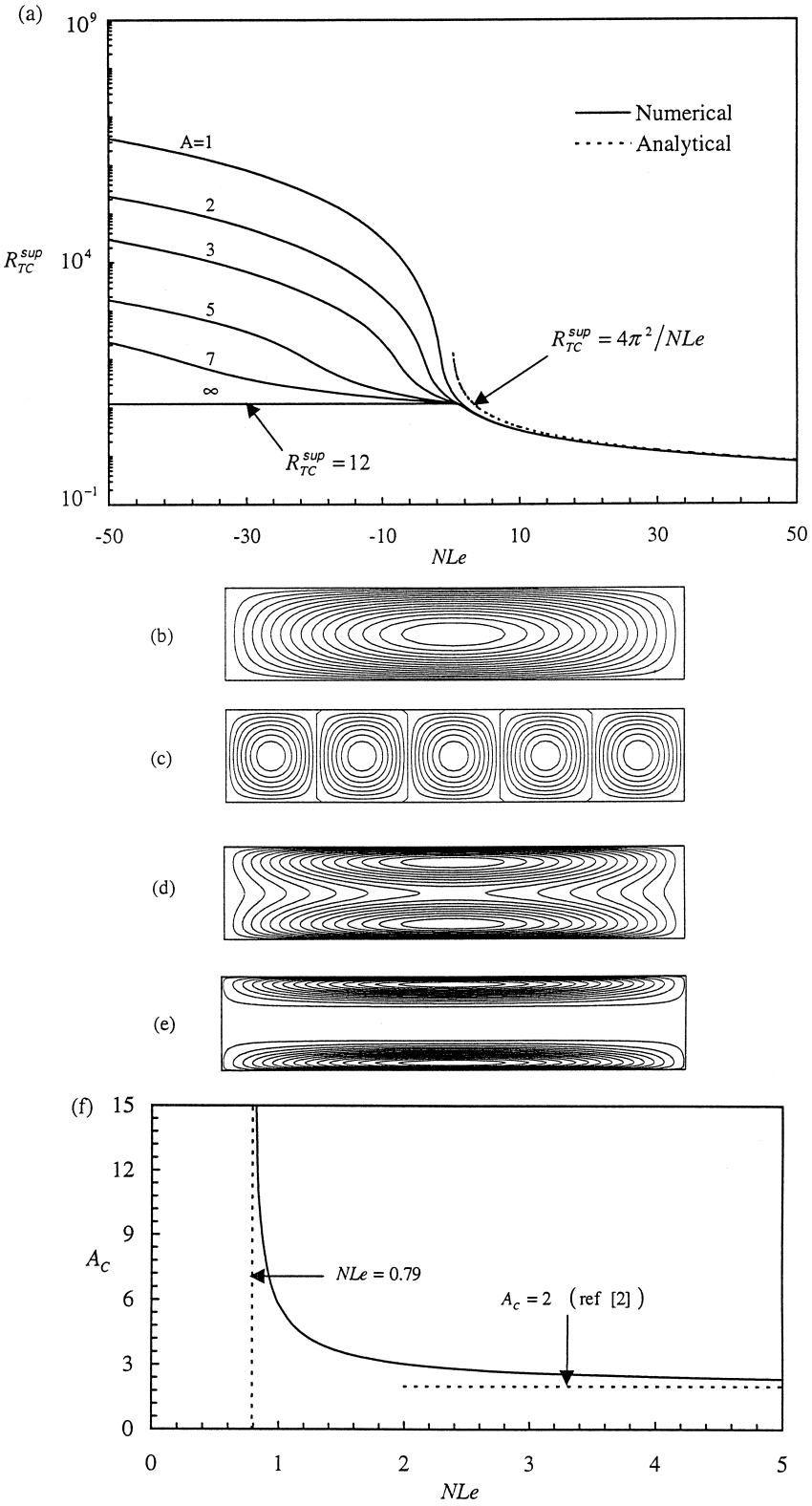

Fig. 3. (a) R_{TC}^{sup} as a function of $N\,Le$ for various values of A and streamline patterns for $A = 5$; (b) $N\,Le = 0$, $R_{TC}^{sup} = 12.45$; (c) $N\,Le = 50$, $R_{TC}^{sup} = 76.37 \times 10^{-2}$; (d) $N\,Le = -25$, $R_{TC}^{sup} = 200.29$; (e) $N\,Le = -50$, $R_{TC}^{sup} = 1715.58$ and (f) effect of $N\,Le$ on the critical wavelength, A_C.

$$R_{TC}^{osc} = a\frac{(Le\,\varepsilon - c)[(\varepsilon - bcN) + 2\sqrt{-\varepsilon bcN}]}{Le(\varepsilon + bcN)^2} \quad (33)$$

From Eqs. (29)–(33) it can be demonstrated that overstable regime exists only for the case of opposing flow ($N < 0$) and more precisely when $R_T > a\varepsilon\ Le/(\varepsilon\ Le - c)$ and $R_S < -ac/b(\varepsilon\ Le - c)$ with the condition $Le \geq c/\varepsilon$. Since $c > 1$ (Fig. 2f) and $\varepsilon < 1$, the Lewis number, Le, must be greater than unity to have overstable regime.

The influence of the aspect ratio A of the cavity on the coefficients a, b and c, Eq. (28), is illustrated in Fig. 2 for various values of $N\ Le$. The results obtained for $N\ Le \geq 0$, for which both temperature and solute gradients are destabilizing, are depicted in Figs. 2a–c. The case $N\ Le = 0$ corresponds to the Rayleigh–Bénard problem with flux boundary conditions for which the flow pattern, at the onset of convection, consists of a single cell occupying the entire cavity (see, for instance, Fig. 3b). For this situation, Fig. 2 indicates a strong dependence of coefficients a, b and c with the aspect ratio of the cavity. On the other hand, the limit $N\ Le \to \infty$ corresponds to the Rayleigh–Bénard problem with Dirichlet boundary conditions. For this situation, the flow within the cavity is possibly multicellular and the resulting number of cells depends essentially upon the aspect ratio of the cavity. In general, at each value of $A = \sqrt{n(n+1)}$ the number of cells increases from n to $(n + 1)$, resulting in a jump of the values of a, b and c. For instance when $A = 1$ we have only cell ($n = 1$) in the cavity. Upon increasing A from unity up to $A = \sqrt{2}$ a one mode cell prevails. Above $A = \sqrt{2}$, the flow exhibits a two-cells mode and this process continues as the value of A is made larger. Naturally, both the strength and the frequency of these jumps are reduced as the value of $N\ Le$ is made smaller. The results obtained for $N\ Le < 0$, for which the temperature gradient is destabilizing and the solute gradient stabilizing, are depicted in Figs. 2d–e. As will be discussed later, the absence of jumps in the curves is due to the fact that for this situation, the flow pattern remains unicellular independently of the values of $N\ Le$ and A.

The supercritical Rayleigh number, R_{TC}^{sup}, is presented in Fig. 3a, as a function of the parameter $N\ Le$, for various values of the aspect ratio, A. Typical streamline patterns are illustrated in Figs. 3b–e for $A = 5$ and various values of $N\ Le$. For $N\ Le > 0$, i.e., when both temperature and solute gradients are destabilizing, the results are observed to be almost independent of the aspect ratio. When $N\ Le$ is sufficiently large, the onset of convection is governed by the solute effects and $R_{TC}^{sup} = 4\pi^2$, as predicted by Lapwood [2], such that $R_{TC}^{sup} = 4\pi^2/N\ Le$. This limit, which is indicated in Fig. 3a by a dotted line, is observed to be reached approximately for $N\ Le \geq 10$. The resulting flow pattern at the onset of convection is illustrated in Fig. 3c for $N\ Le = 50$ where five counter rotating cells are present in the cavity. This situation corresponds to the classical Bénard problem. The case $N\ Le < 0$ will now be discussed. For this situation the flux component (temperature) is destabilizing while the fixed-value component (solute) is stabilizing. In general, Le is greater than unity such that the resulting situation is analogous to the diffusive regime of conventional thermohaline convection where the faster diffusing component is destabilizing and the slower diffusing component is stabilizing. The results depicted in Fig. 3a indicate that, for a given value of A, R_{TC}^{sup} increases monotonously as the value of $N\ Le$, that is the strength of the solutal stabilizing gradient, is enhanced. However, it is observed that, for a slender enclosure ($A = \infty$), $R_{TC}^{sup} = 12$ independently of the value of $N\ Le$ when this later is below 0.79. This result indicates that, in an infinite horizontal layer, the onset of convection is independent of the magnitude of the stabilizing gradient. The resulting situation corresponds to the Rayleigh–Bénard problem with flux boundary conditions for which the primary instability occurs at zero horizontal wave number. Similar results have been reported in the past by Nield [19] and Tsitverblit [20] while considering double-diffusive convection in a horizontal fluid layer subject to mixed boundary conditions. With the boundary conditions considered by Tsitverblit [20] the fixed-value component (heat) was stabilizing such that his problem is analogous to the finger regime of thermohaline convection as opposed to the analogy of the problem considered here with the diffusive regime. The effects of negative values of $N\ Le$ on the flow patterns at the onset of convection are illustrated in Figs. 3d–e. For $N\ Le = -25$, Fig. 3d indicates the existence of two superposed co-rotating long cells filling up the entire cavity. As the value of $N\ Le$ is decreased these two cells move progressively toward the upper and lower boundaries and the core region becomes motionless. Thus, for $N\ Le = -50$, Fig. 3e shows the presence of very thin cells at the vicinity of the two horizontal boundaries. This flow behavior is due to the confinement of the enclosure and it does not appear for an infinity layer. Fig. 3f illustrates the effect of the parameter $N\ Le$ on the wavelength A_C of the incipient flow structure induced within an infinite layer ($A \to \infty$). According to the linear stability theory for $N\ Le = < 0.79$, *the flow remains unicellular* ($A_C = \infty$) independently of the strength of the stabilizing solutal gradient. For $N\ Le > 0.79$ the flow structure is multicellular and A_C decreases from infinity toward the classical value $A_C = 2$ predicted by Lapwood [2] for a porous layer saturated by a monocomponent fluid ($N\ Le \to \infty$).

Typical stability diagrams, as predicted by the linear stability theory, are illustrated in Fig. 4a–b for the cases of a square enclosure ($A = 1$) and an infinite

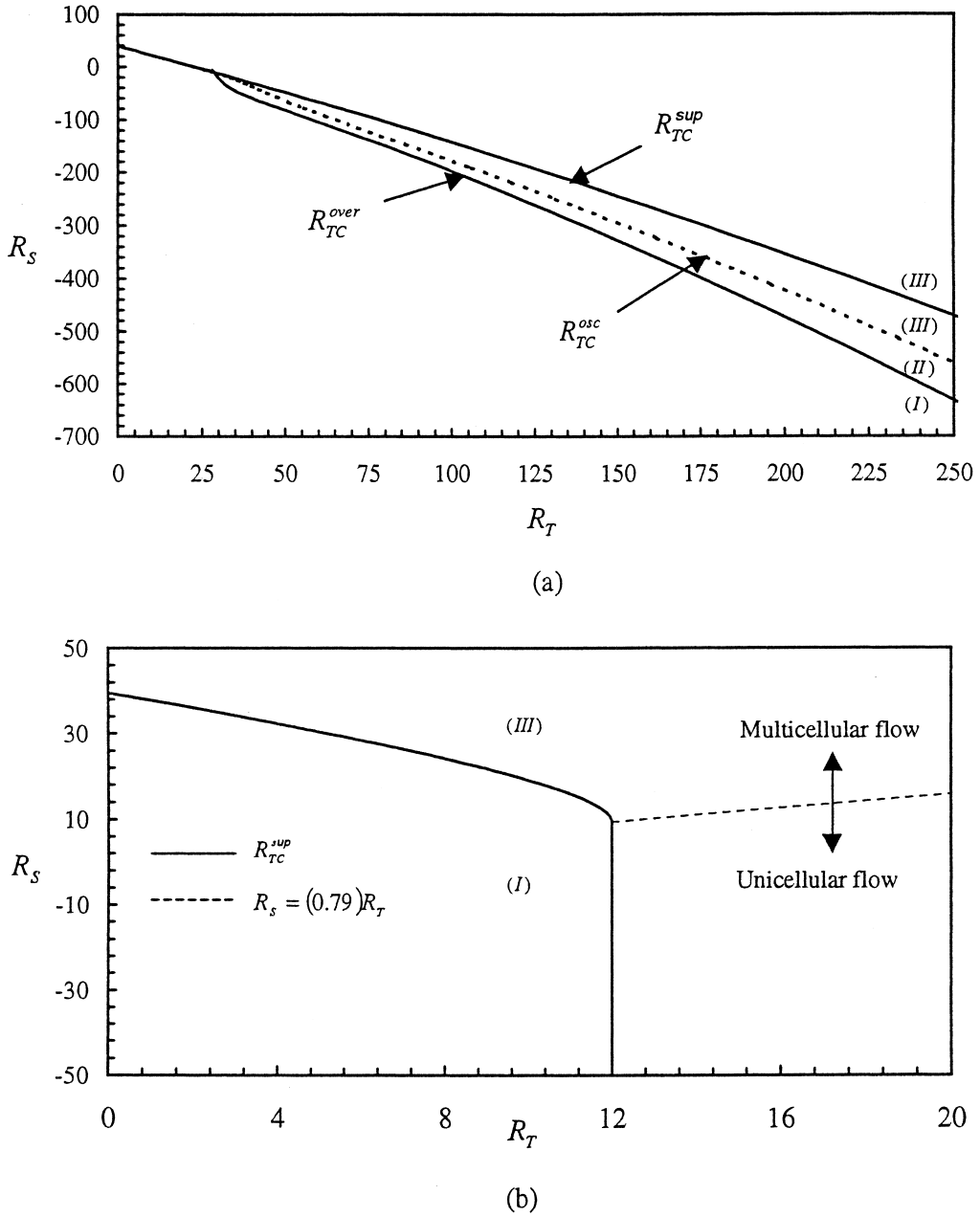

Fig. 4. Stability diagrams for $Le = 10$ and $\varepsilon = 1$; (a) $A = 1$ and (b) $A = \infty$.

layer ($A = \infty$), respectively. The results are presented in the R_T–R_S plane for $Le = 10$ and $\varepsilon = 1$. For a square enclosure ($A = 1$), three distinct regions delimited by the curves corresponding to Eqs. (29), (32) and (33) are observed to exist (see Fig. 4a). In Region I, $R_T < R_{TC}^{over}$, the basic rest state solution is stable according to the linear stability theory. This point was confirmed by the numerical simulation of the full governing equations that will be discussed in the next section. In region II, $R_{TC}^{over} < R_T < R_{TC}^{osc}$, the linear stability analysis shows that both real and imaginary parts of the parameter, p, Eqs. (30) and (31), are positive. In this region the numerical results indicate that upon starting the numerical runs with the rest state as initial conditions, the flow, temperature and concentration amplitudes grow with time in an oscillatory manner. In region III ($R_T > R_{TC}^{osc}$), above the neutral stability line, the system is unstable and all the numerical results

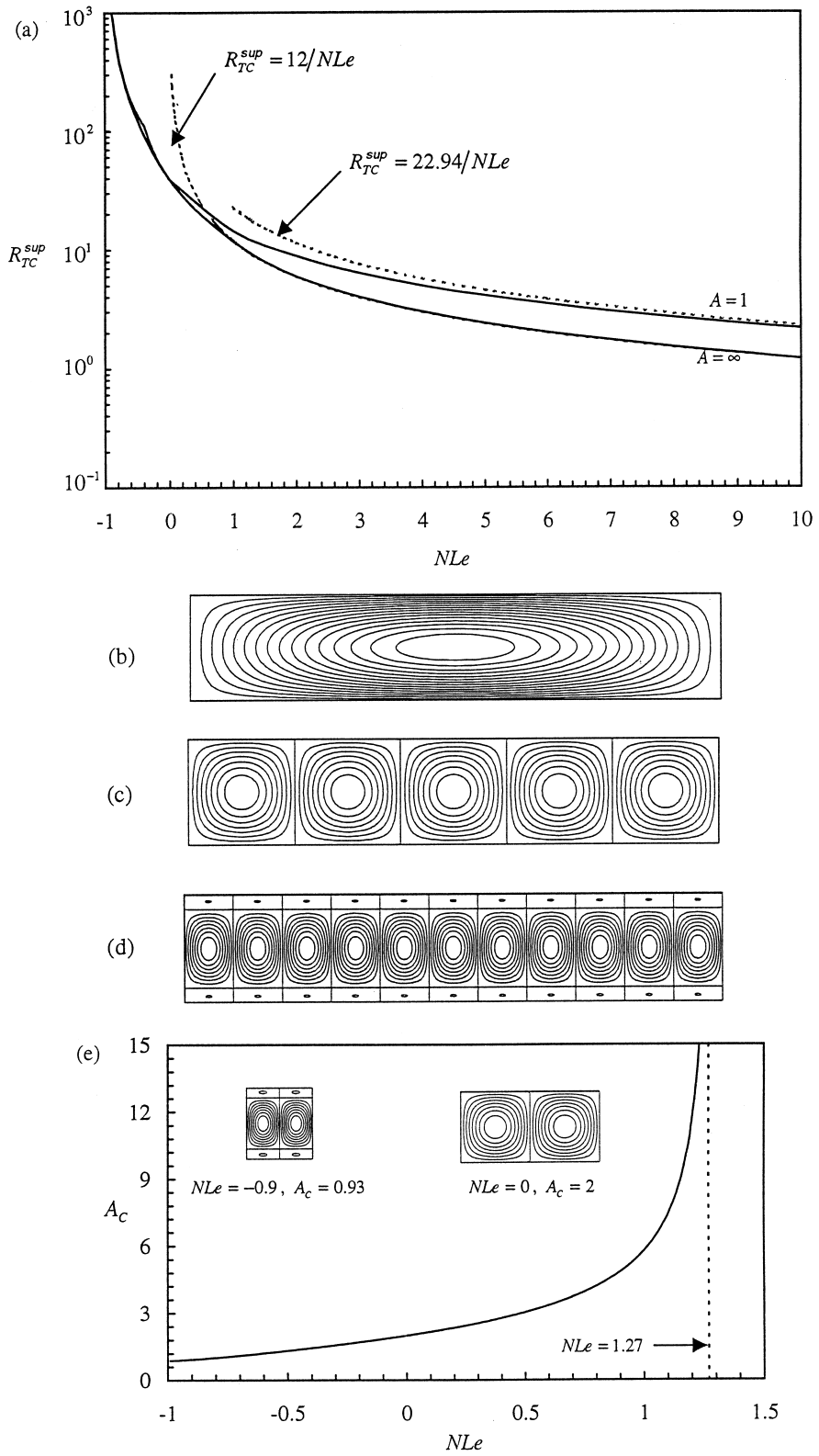

Fig. 5. Results obtained for the case of Dirichlet thermal and Neumann solutal boundary conditions: (a) R_{TC}^{sup} as a function of $N\,Le$ for various values of A and streamline patterns for $A = 5$; (b) $N\,Le = 50$, $R_{TC}^{sup} = 24.88 \times 10^{-2}$; (c) $N\,Le = 0$, $R_{TC}^{sup} = 39.85$; (d) $N\,Le = -0.9$, $R_{TC}^{sup} = 1049.69$ and (e) effect of $N\,Le$ on the critical wavelength, A_C.

obtained in this region demonstrated the existence of finite amplitude convection, independently of the initial conditions. However, for an infinite layer (see Fig. 4b), the principle of exchange of stability is valid and overstable regimes are not possible. For this case the rest state solution becomes unstable only when $R_T > R_{TC}^{sup}$. The transition between unicellular and multicellular flows is given by the relation $R_S = 0.79 R_T$ indicated as a dotted line on the graph.

All the above results are concerned with the case where the destabilizing gradient of temperature is specified by the heat flux applied on the horizontal boundaries and the stabilizing ($N\,Le < 0$) gradient of solute by the difference in its values between these boundaries. For completeness, the same problem was considered for the case when temperature and concentration on the boundaries are specified in terms of the fixed-value and flux boundary conditions, respectively. Fig. 5 shows the results obtained, following the numerical technique described before (the only difference being in the boundary conditions). As it can be seen by comparing Figs. 3 and 5, the instability mechanism is considerably affected by the specifications of the boundary conditions of the stabilizing and destabilizing components.

In Fig. 5a, R_{TC}^{sup} is plotted as a function of $N\,Le$ for $A = 1$ and ∞. With the boundary conditions considered here when $N\,Le$ is large enough, the onset of convection is induced by the destabilizing solutal gradient maintained by the flux conditions. The resulting flow pattern for this situation is unicellular (see for instance Fig. 5b for $A = 5$) and $R_{SC}^{sup} = 22.94$ (12) when $A = 1$ (∞) such that $R_{TC}^{sup} = 22.94/N\,Le$ ($12/N\,Le$). These two asymptotic limits are depicted by dotted lines in Fig. 5a. It is found that the solutal gradients are predominant for $N\,Le \geq 10$, when $A = 1$ and $N\,Le \geq 1$ when $A = \infty$. As the value of $N\,Le$ is reduced down to $N\,Le = 0$ the resulting situation corresponds to the Bénard problem for which the linear stability theory predicts that for $R_{TC}^{sup} = 4\pi^2$ instability appears as convection in the form of rolls of square vertical cross section. This point is illustrated in Fig. 5c which shows the existence of five counter-rotating rolls in a cavity of aspect ratio $A = 5$. With the boundary conditions considered here when $N\,Le \leq 0$, the flux component solute is stabilizing and the fixed value component (temperature) is destabilizing. For this situation Fig. 5a indicates that R_{TC}^{sup} increases asymptotically towards infinity as the value of $N\,Le \rightarrow -1$. According to the linear stability theory, when $N\,Le \leq -1$, the system is unconditionally stable. Fig. 5d shows the flow pattern obtained for $N\,Le = -0.9$ for which 11 counter-rotating cells are now present in the cavity. The presence of secondary cells near the horizontal boundaries is also observed. For an infinite layer ($A = \infty$) the effect of $N\,Le$ on the critical wavelength is depicted in Fig. 5e. It is observed that the flow is unicellular when $N\,Le > 1.27$. The critical wavelength A_C decreases from infinity to 0.87 as the value of $N\,Le$ is decreased from 1.27 to -1. For $N\,Le < 0$; for instance $N\,Le = -0.9$, $A_C = 0.93$ and the flow patterns consists of two main counter-rotating cells squeezed by two small vortices located near the upper and the lower boundaries as illustrated in Fig. 5e.

6. Finite amplitude convection

In order to study the effect of a combination of the flux and fixed-value boundary conditions on the development of finite amplitude double-diffusive convection, the full governing Eqs. (2)–(4), with the associated boundary conditions (7), were solved numerically by a finite difference method. The energy and concentration equations were solved using the time-marching finite difference technique. The first and second derivatives were approximated by central differences and time derivative by a first-order backward discretization. The discretized forms of the energy and concentration equations was written in conservative form for the nonlinear convection terms in order to preserve the conservation property. Eq. (2) was solved by the Successive-Over-Relaxation method. The iterative procedure was carried out until a steady-state was obtained. The convergence criteria for all field variables are $|\phi_{new} - \phi_{old}|_{ext} \leq 10^{-10}$, where ϕ stands for any field variables and the subscript 'ext' denotes extremum value over the grid points. As a result of a grid independence study, grid size of 80×80 is chosen for the majority of the calculations. The time step was selected so that no numerical oscillations occurred. During the iterations, the field always evolved smoothly from arbitrary initial data to final steady states. The accuracy of the numerical model was verified by comparing results from the present investigation with those reported by Kimura et al. [18] for the case of a shallow cavity heated from below by a constant heat flux ($N = 0$). Maximum differences between the two investigations were within 0.5%.

The local heat and mass fluxes at the walls are given in dimensionless terms by the Nusselt and Sherwood numbers which can be evaluated, respectively, by

$$Nu = \frac{q'}{k\overline{\Delta T'}/H'} = \frac{1}{\Delta T}; \quad Sh = \left.\frac{\partial S}{\partial y}\right|_{y=\pm 1/2} \tag{34}$$

where $\Delta T = T(x, -1/2) - T(x, +1/2)$ is the side-to-side dimensionless temperature difference.

Integrating the results for local Nusselt and Sherwood numbers along the horizontal walls yields the results for the overall Nusselt and Sherwood numbers as

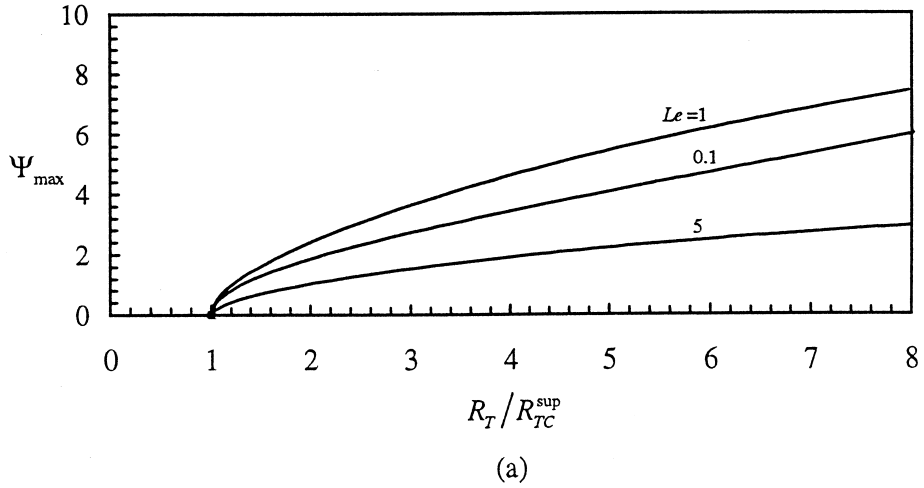

(a)

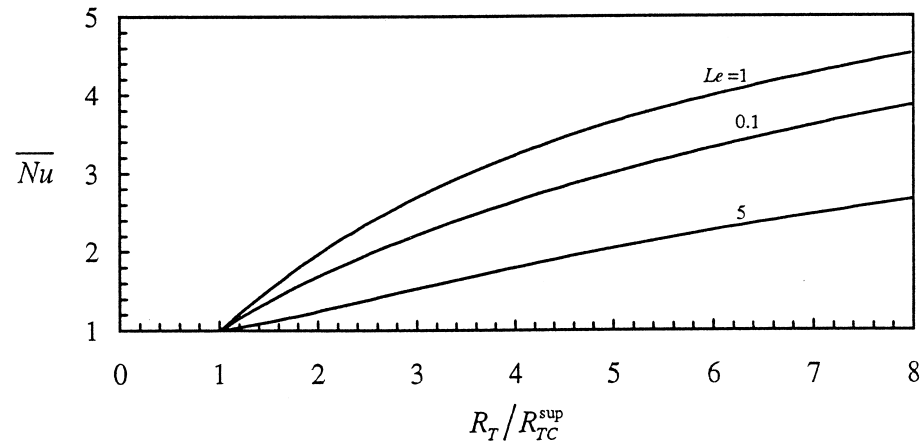

(b)

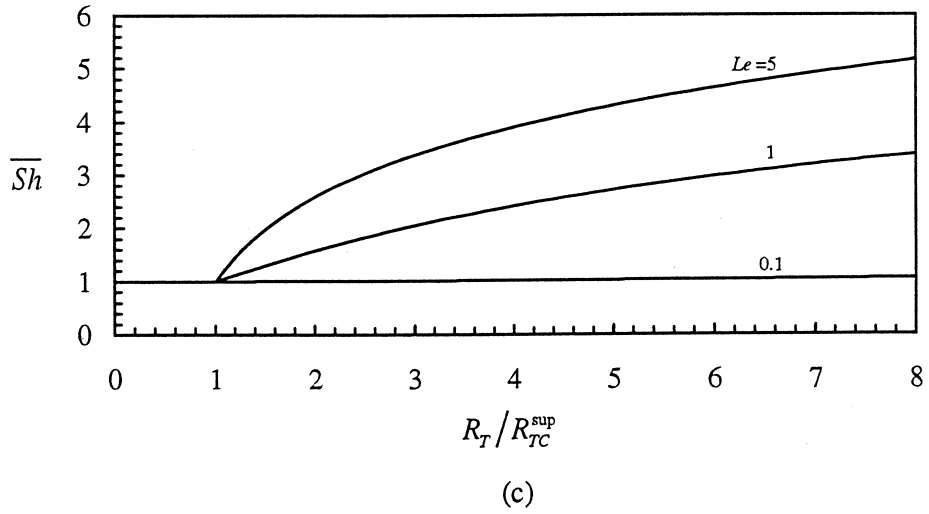

(c)

Fig. 6. Bifurcation diagram for $A = 1$, $N = 1$ and $Le = 0.1$, 1 and 5, respectively: effect of the thermal Rayleigh number on (a) Ψ_{max}, (b) $\overline{Nu}$ and (c) $\overline{Sh}$.

$$\overline{Nu} = \frac{1}{A}\int_{-A/2}^{A/2} Nu\,\mathrm{d}x; \quad \overline{Sh} = \frac{1}{A}\int_{-A/2}^{A/2} Sh\,\mathrm{d}x \tag{35}$$

The effect of the thermal Rayleigh number on the maximum value of the stream function Ψ_{max} and on Nusselt and Sherwood numbers $\overline{Nu}$ and $\overline{Sh}$ are illustrated on Fig. 6 for $A = 1$, $N = 1$, $Le = 0.1$, 1 and 5 ($R_{TC}^{sup} = 21.70$, 14.56 and 5.89, respectively). For $N > 0$, i.e., for aiding double-diffusive flow, both thermal and solutal buoyancy forces are destabilizing and the graph illustrates a standard supercritical bifurcation as it exists for the classical Bénard problem. Any perturbation brought to the system at $R_T/R_{TC}^{sup} < 1$ is resorbed. Fig. 6 also shows that the Sherwood number increases as the Lewis number is made larger. This follows from the fact that, as the Lewis number is increased, the diffusivity of the solute becomes relatively less important than that of heat, thus promoting the intensity of the mass transfer. For the same reason, it is observed that, excepted for the case $Le = 0.1$, the Nusselt number decreases with the Lewis number. In Fig. 7 the influence of the Lewis number is also illustrated for $A = 1$ and $R_T/R_{TC}^{sup} = 4$ in terms of the streamlines (top), isotherms (center) and iso-concen-

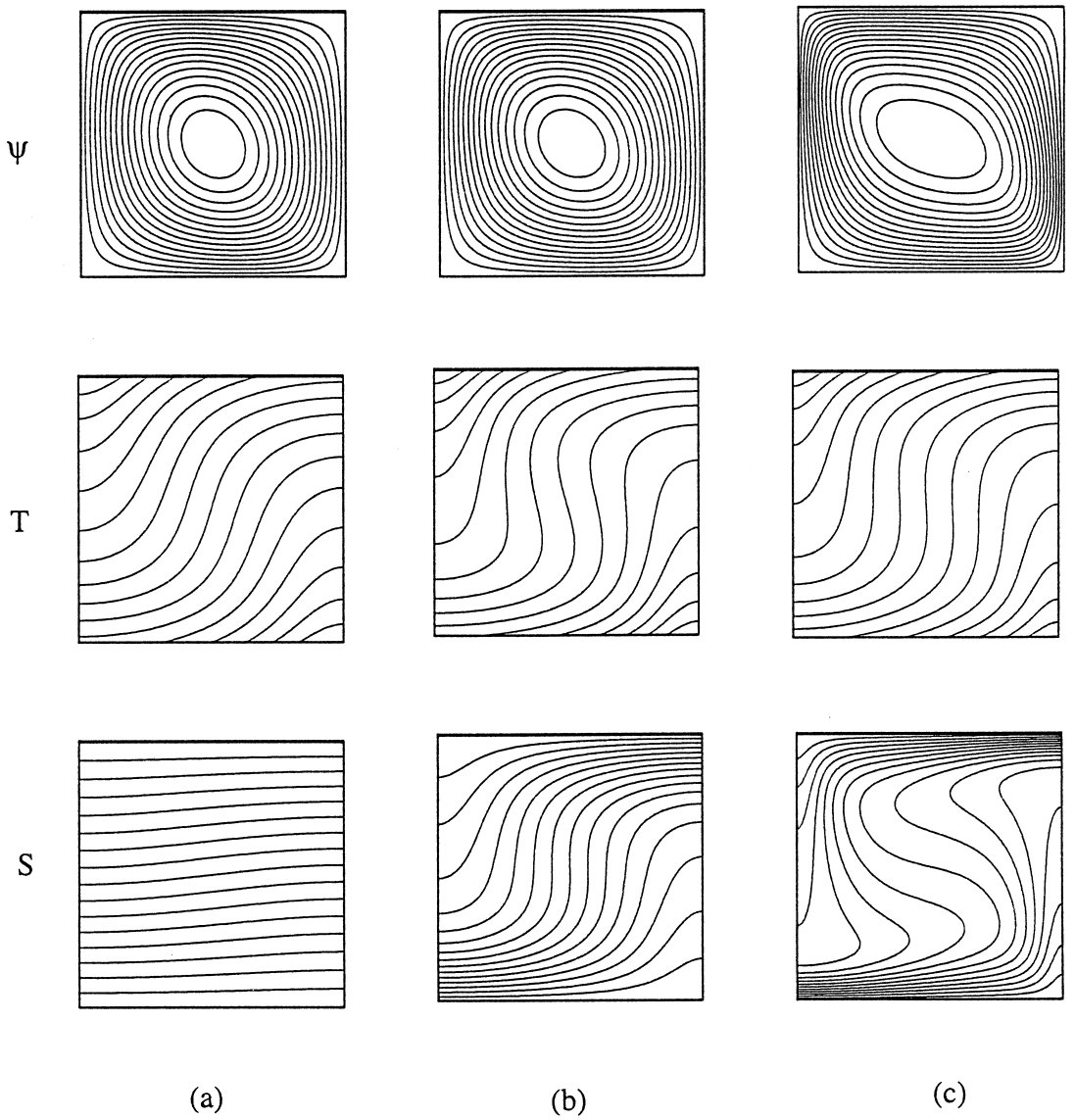

Fig. 7. Stream function, temperature and concentration fields for $A = 1$, $N = 1$, $R_T/R_{TC}^{sup} = 4$ and (a) $Le = 0.1$, $\Psi_{max} = 3.42$, $\overline{Nu} = 2.64$, $\overline{Sh} = 1.02$, (b) $Le = 1$, $\Psi_{max} = 4.61$, $\overline{Nu} = 3.23$, $\overline{Sh} = 2.42$ and (c) $Le = 5$, $\Psi_{max} = 1.91$, $\overline{Nu} = 1.78$, $\overline{Sh} = 3.90$.

tration (bottom). The intervals of streamlines, isotherms and iso-concentrations are $|f_{max}-f_{min}|/16$, where f stands for Ψ, T and S. All these results indicate that, for a given Rayleigh number, upon increasing Le from 0.1 to 5, both Ψ_{max} and $\overline{Nu}$ are observed to first increase with Le up to $Le=O(1)$ and then to decrease. The mass transfer, on the other hand is seen to be a decreasing function of Le, as this parameter is reduced toward zero.

The effect of R_T on the flow intensity Ψ_{max} is illustrated on Fig. 8a for the case $A = 1$, $Le = 10$, $\varepsilon=1$ and $N=-0.1$, i.e., for opposing double-diffusing flow.

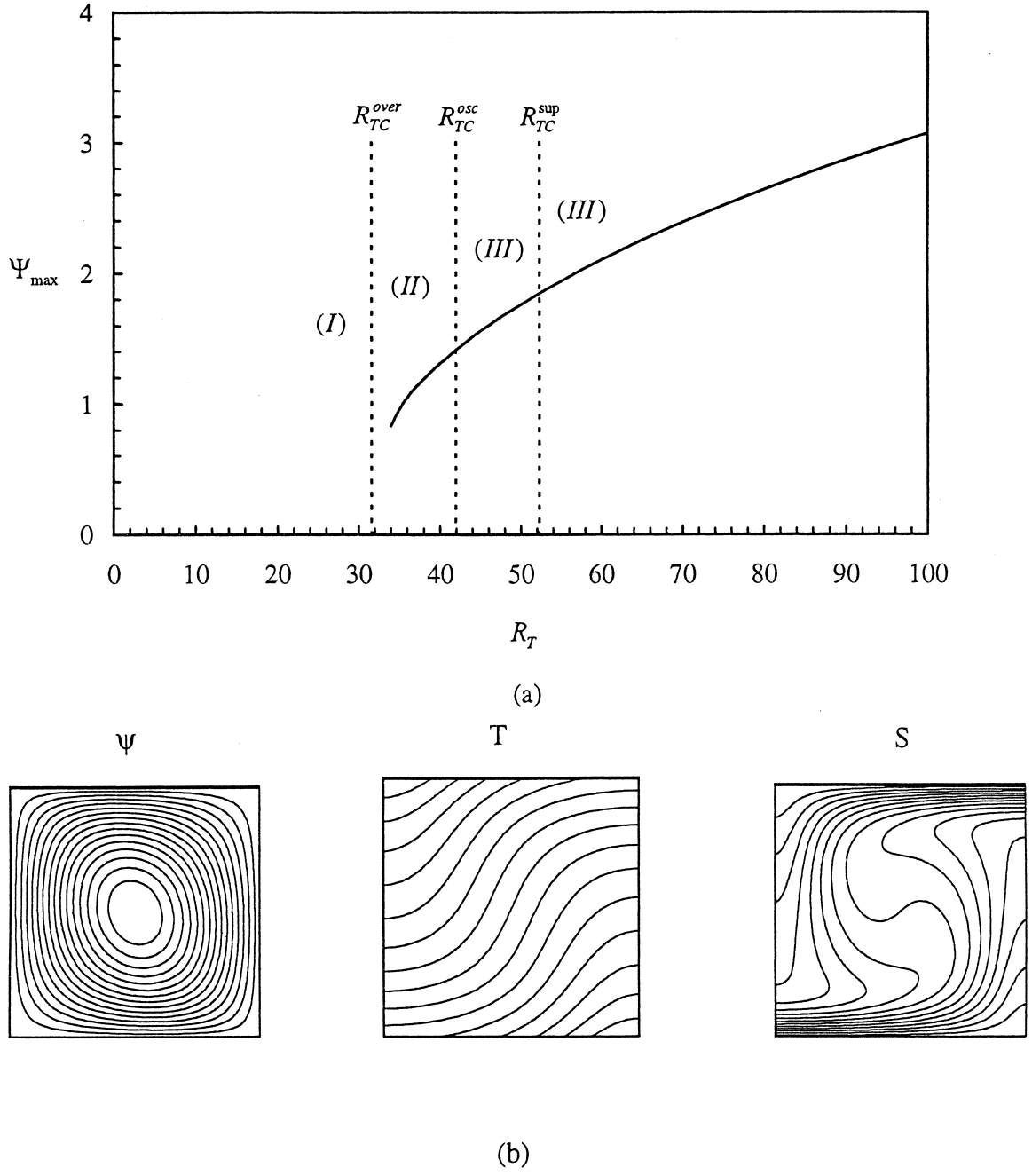

Fig. 8. (a) Bifurcation diagram and (b) stream function, temperature and concentration fields for $R_T=R_{TC}^{sup}=52.23$ for the case $A = 1$, $Le = 10$, $\varepsilon=1$ and $N=-0.1$, $\Psi_{max}=1.85$, $\overline{Nu}=1.63$ and $\overline{Sh}=5.15$.

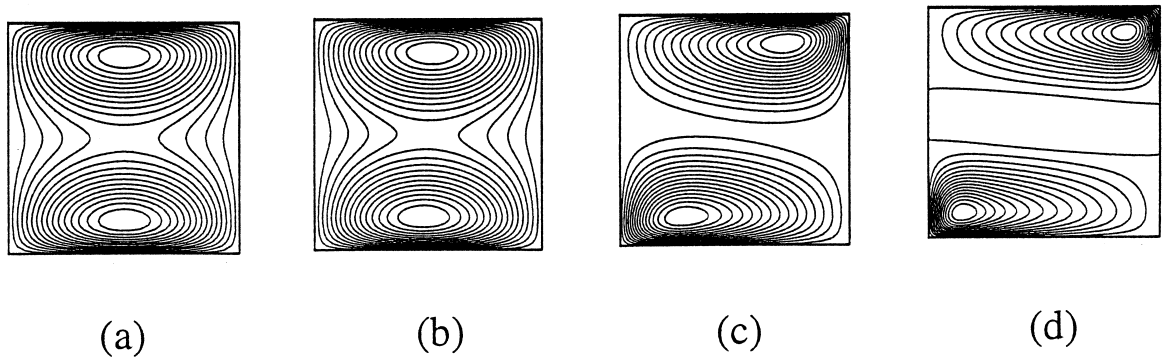

Fig. 9. Flow patterns obtained for $A = 1$ and $N\,Le = -2$; (a) $R_T = R_{TC}^{sup} = 307.35$ (incipient flow); (b) $R_T = 310$, $\Psi_{min} = 0$, $\Psi_{max} = 0.056$, (c) $R_T = 500$, $\Psi_{min} = 0$, $\Psi_{max} = 0.641$ and (d) $R_T = 1000$, $\Psi_{min} = -0.091$, $\Psi_{max} = 1.356$.

According to the linear stability theory it is found that $R_{TC}^{sup} = 52.23$, $R_{TC}^{over} = 31.58$ and $R_{TC}^{osc} = 42.96$. The solid lines in the graph represents the results of the present numerical simulation. These results, for a given R_T, were obtained by starting the numerical simulation with a finite amplitude flow obtained at a higher Rayleigh number, as initial conditions. In this way it was found that convection was possible down to a value of $R_T = 35$, that is well below the supercritical Rayleigh number $R_{TC}^{sup} = 52.23$. For $R_{TC}^{over} < R_T < 35$, the convective flow was found to oscillate. Thus, Fig. 8a illustrates a subcritical bifurcation for which there exists a subcritical Rayleigh number at which a stable convective solution bifurcates from the rest state through finite-amplitude convection. In general, a non linear stability is necessary to predict this critical Rayleigh number (see, for instance, Ref. [21]) The flow field and its corresponding temperature and solute fields, obtained at $R_T = R_{TC}^{sup} = 52.23$ is shown in Fig. 8b. The isotherms and isoconcentration are observed to be strongly distorted at the onset of supercritical convection, this behavior being typical of a subcritical bifurcation.

For a square enclosure finite amplitude results are obtained for $N\,Le = -2$. The results are depicted in Fig. 9 in terms of flow patterns obtained for various values of the Rayleigh number. According to the linear stability analysis, it is found that $(1 + bN\,Le) > 0$ since $b = 0.38$ when $N\,Le = -2$. Thus, for this situation, the only possible bifurcation is the supercritical one. For that reason, finite amplitude numerical solution indicates no flow motion for $R_T \leq R_{TC}^{sup} = 307.35$. At the onset of convection, as shown in Fig. 9a, the flow pattern exhibits two superposed co-rotating cells surrounded by the main flow circulation. At the vicinity of the threshold (i.e., $R_T = 310$), a good agreement is found between the finite amplitude results, Fig. 9b, and the linear stability analysis prediction, Fig. 9a. As the Rayleigh number is increased above R_{TC}^{sup}, the main flow disappears gradually and the co-rotating cells move progressively towards the horizontal boundaries as illustrated in Fig. 9c for $R_T = 500$. For $R_T = 1000$, Fig. 9d shows that the flow is now concentrated in the bottom right and the top left corners of the cavity. Also, it is observed that a weak counter-rotating cell is generated in the central part of the enclosure.

7. Conclusion

The onset of double-diffusive convection in a rectangular porous cavity, with mixed boundary conditions for heat and solute applied on the horizontal boundaries, has been studied numerically. The stability to small perturbations from the rest state has been investigated using a linear stability theory. A finite difference method was used to simulate finite amplitude convective flows. The main findings of the present investigation are

1. Temperature and concentration specified in terms of Neumann and Dirichlet boundary conditions, respectively:
   1.1. For aiding flows ($N\,Le > 0$) the results of the linear stability theory indicate that the supercritical Raleigh number R_{TC}^{sup} depends strongly upon the buoyancy ratio parameters $N\,Le$ and the aspect ratio of the enclosure A. For an infinite layer (the critical wavelength $A \to \infty$) when $0 < N\,Le < 0.79$ the flow remains unicellular ($A_C \to \infty$) and $R_{TC}^{sup} = 12$. For $N\,Le > 0.79$ the flow is multicellular and for solute driven flow ($N\,Le \gg 1$) R_{TC}^{sup} and A_C tends toward the classical values $4\pi^2/N\,Le$ and 2, respectively. For finite amplitude convection it was found numerically that the heat and mass transfer rates, Nu and Sh, are different from each other even when $Le = 1$.

1.2. For opposing flows ($N\ Le < 0$) and a given aspect ratio A it is found that R_{TC}^{sup} increases as $N\ Le \to -\infty$. For this situation, the incipient flow patterns consists of two co-rotating long cells located in the vicinity of the horizontal boundaries. The existence of subcritical convection and oscillatory modes has been demonstrated. For an infinite layer ($A \to \infty$), $R_{TC}^{sup} = 12$ and the flow remains unicellular ($A_C \to \infty$) independently of $N\ Le$, i.e., the strength of the stabilizing concentration gradient. For this situation oscillatory convection is not possible.

2. Temperature and concentration specified in terms of Dirichlet and Neumann boundary conditions, respectively: according to the linear stability analysis the rest state is unconditionally stable for $N\ Le \leq -1$. For $-1 < N\ Le < 1.27$ the flow is multicellular and the critical wavelength depends upon the parameter $N\ Le$. For $N\ Le > 1.27$ the flow is unicellular ($A_C \to \infty$). For $-1 < N\ Le < 0$ overstability and subcritical convection are expected to occur.

Acknowledgements

This work was supported in part by the Natural Sciences and Engineering Research Council, Canada and jointly by the FCAR, Government of Quebec.

References

[1] C.W. Horton, F.T. Rogers, Convection currents in a porous medium, Journal of Applied Physics 16 (1945) 367–370.
[2] E.R. Lapwood, Convection of a fluid in a porous medium, Proceeding of Cambridge Philosophical Society 44 (1948) 508–521.
[3] D.A. Nield, A. Bejan, Convection in Porous Media, 2nd ed., Springer-Verlag, 1999.
[4] D.A. Nield, Onset of thermohaline convection in porous medium, Water Resources Research 4 (1968) 553–560.
[5] J.W. Taunton, E.N. Lightfoot, Thermohaline instability and salt fingers in a porous medium, Physics of Fluids 15 (1972) 748–753.
[6] D. Poulikakos, Double diffusive convection in a horizontal sparsely packed porous layer, International Communications in Heat Mass Transfer 13 (1986) 587–598.
[7] M.S. Malashetty, Anisotropic thermoconvective effects on the onset of double diffusive convection in a porous medium, International Journal of Heat and Mass Transfer 39 (1993) 2397–2401.
[8] N. Rudraiah, P.K. Srimani, R. Friedrich, Finite amplitude convection in a two-component fluid saturated porous layer, International Journal of Heat and Mass Transfer 25 (1982) 715–722.
[9] H. Brand, V. Steinberg, Nonlinear effect in the convective instability of a binary mixture in a porous medium near threshold, Physics Letters 93 (A) (1983) 333–336.
[10] O.V. Trevisan, A. Bejan, Mass and heat transfer by high Rayleigh number convection in a porous medium heated from below, International Journal of Heat and Mass Transfer 30 (1987) 2341–2356.
[11] B.T. Murray, C.F. Chen, Double-diffusive convection in a porous medium, Journal of Fluid Mechanics 201 (1989) 147–166.
[12] N.D. Rosenberg, F.J. Spera, Thermohaline convection in a porous medium heated from below, International Journal of Heat and Mass Transfer 35 (1992) 1261–1273.
[13] F. Chen, C.F. Chen, Double-diffusive fingering convection in a porous medium, International Journal of Heat and Mass Transfer 36 (1993) 793–807.
[14] M. Mamou, P. Vasseur, E. Bilgen, D. Gobin, Double-diffusive convection in an inclined slot filled with porous medium, European Journal of Mechanics, B/Fluids 14 (1995) 629–652.
[15] T.H. Nguyen, T.H. Tran, P. Vasseur, Double-diffusive convection in a porous layer: fluid flow and contaminant transport in groundwater. Proceeding of the International Conference Engineering Mechanics Today EMT 1997 Hanoi, Vietnam, 1997.
[16] A. Mahidjiba, Convection naturelle thermosolutale au sein d'une couche poreuse horizontale. M.Sc.A thesis, École Polytechnique, University of Montreal, Canada, 1998.
[17] M. Mamou, P. Vasseur, E. Bilgen, A. Galerkin, A Galerkin finite element study of the onset of double-diffusive convection in an inclined porous enclosure, International Journal of Heat and Mass Transfer 41 (1998) 1513–1529.
[18] S. Kimura, M. Vynnycky, F. Alavyoon, Unicellular natural circulation in a horizontal porous layer heated from below by a constant flux, Journal of Fluid Mechanics 294 (1995) 231–257.
[19] D.A. Nield, The thermohaline Rayleigh–Jeffrey problem, Journal of Fluid Mechanics 29 (1967) 545–556.
[20] N.A. Tsitverblit, On the nature of direct instability in double-component convection with different boundary conditions, Physics of Fluids 9 (1997) 10–14.
[21] M. Mamou, P. Vasseur, E. Bilgen, Double-diffusive convection instability in a vertical porous enclosure, Journal of Fluid Mechanics 368 (1998) 263–289.